









Research Article

UIR: Implementing Deep Neural Networks in addition to Conventional Algorithms for Ultra-Image Recovery

Ali Salim Rasheed^{1,*}, Alaa Hamza Omran², Mohammad Aljanabi³, Mohammed Almaaya⁴, Rami Sheha⁵,
Mansour Obeidat⁶, Theyazn H. H. Aldhyani⁷, Mosleh Hmoud AlAdhaileh⁶

¹Department of Media Technology and Communications Engineering, College of Engineering, University of Information Technology and Communications, Baghdad, Iraq

²Ministry of Higher Education and Scientific Research, Baghdad, Iraq

³Technical Engineering College, Imam Ja'afar Al-Sadiq University (IJSU), Baghdad, Iraq

⁴King Abdullah the II IT School, The University of Jordan, Amman, Jordan

⁵Vice-Presidency for Postgraduate Studies and Scientific Research, King Faisal University, Al-Ahsa 31982, Saudi Arabia

⁶Applied College, King Faisal University, Al-Ahsa, Saudi Arabia

⁷Deanship of E-Learning and Distance Education and Information Technology, King Faisal University, Al-Ahsa, Saudi Arabia

ARTICLE INFO

Article History

Received 19 Jan 2025

Revised 31 Jul 2025

Accepted 15 Aug 2025

Published 23 Aug 2025

Keywords

Deep conventional
neural networks

Superresolution

High-dimensional
vector

Residual Swin
Transformer block



ABSTRACT

Many of the images that can be accessed through web search engines or social media networking sites are rare and not high quality because they are endangered or disappear. There must be a way to increase the quality of these images and conduct experiments to reduce noise, remove blur, and make them sharper to reach high-quality surfaces. Approaches that seek to achieve better results compete to increase the efficiency of those low-resolution images and generate images with the same color (RGB) characteristics but with higher quality. Deep learning algorithms, especially the use of convolutional neural networks (CNNs), have achieved advanced results within this context. In this approach, we propose a powerful base model UIR for image recovery by using conventional neural networks (CNNs) added to conventional algorithms for ultra-super-resolution from low-resolution images by extracting the feature map from a low-resolution image I_{LR} as overlapping superresolution I_{SR} patches, in which every patch represents a high-dimensional vector. The missing features of the pixels that occur during the training process are subsequently compensated via the residual Swin Transformer block (RSTB). The results of quantitative evaluation experiments using PSNR(db)/SSIM metrics were superior to those of state-of-the-art methods on benchmark datasets (Set5, Set14, and BSD100). The selected images have a magnification of x2, resulting in values of (36.86(db)/0.9739, 36.10(db)/0.9656, 34.74(db)/0.9893) and x4, resulting in values of (34.44(db)/0.9784, 27.71(db)/0.8894, and 26.87(db)/0.9915, respectively. The results of the visual comparison also revealed that the texture of the surfaces is sharper, more expressive, less noisy, and blurry than those of the other methods.

1. INTRODUCTION

Many research approaches have demonstrated the importance of deep learning in recovering high-quality images from low-quality images. Deep learning algorithms have achieved superior technical performance in restoring rough surfaces of damaged or low-resolution images. In addition, deep learning can develop more complex models to handle image degradation scenarios [1]. Deep learning has many applications in image recovery, including in the fields of imaging, medical imaging, and surveillance [2]. By harnessing the power of deep learning, image reconstruction can be performed more effectively and efficiently than ever before. Deep image restoration is the process of recovering high-quality images from damaged input images. Image degradation can be caused by various factors, such as blur, noise, or low resolution [3]. The restoration process involves estimating a clean original image from a damaged copy via deep learning techniques, specifically deep convolutional neural networks. Deep photo recovery is a form of photo recovery that uses deep learning methods to create high-quality images [4].

*Corresponding author. Email: ali.rasheed@uoitc.edu.iq

Several methods [5] rely on the reconstruction of high-resolution patches from low-resolution images by overlapping patches. A low-resolution dictionary then encodes these patches. The final output is reconstructed by overlaying overlapping patches that rely on effective depth mapping to build functionality through a unified framework [6]. These methods, which rely on recovering superresolution images from low-resolution images, learn to find maps from both external low- and high-resolution 2D image pairings on the basis of the similarity of internal properties [7] and the training examples supplied by the datasets [8]. We name our proposed method image recovery via deep conventional neural network conventional algorithms. The primary concept is based on the use of two specialized convolutional neural networks in the superresolution of 2D images.

First, the feature map from a low-resolution image ILR is extracted as overlapping superresolution ISR patches, in which every patch represents a high-dimensional vector by learning deep convolutional neural networks (CNNs) to map between LR/HR 2D images. Once the patches are extracted, they are represented as high-dimensional vectors. This is achieved by using a deep neural network to map between low-resolution and high-resolution 2D images. CNNs have been shown to effectively learn complex mappings between two image types, leading to more accurate feature extraction [9][10]. High-dimensional vector representations of patches allow for more efficient processing and analysis of features [11]. Overall, training deep CNNs to extract features from low-resolution images is a complex process that requires careful consideration of architecture selection, dataset selection, and fine-tuning. However, with the right approach, CNNs can efficiently extract high-dimensional feature vectors from overlapping high-resolution patches, allowing the creation of high-quality images from low-resolution inputs [12][13]. Second, we adopt a logical method for strengthening the basic features of the low-resolution 2D image via deep learning networks to ensure that the missing features of pixels that occur during the training process are compensated via the residual Swin Transformer block (RSTB).

Research progress in supervised self-learning has effectively supported image restoration models by reconstructing textures and correcting dimensions in a manner that mimics their original structure. Multiple mask techniques are used to remove spatial noise correlations that accompany training stages, achieving high accuracy and noise reduction in realistic sRGB images. Moreover, transformer-based methods (such as SwinIR) and modular diffusion strategies address texture restoration by modelling global contexts. These approaches overcome the limitations of scarce or missing datasets in supervised self-learning and enable real-time handling of complex degradations—critical for advanced medical imaging applications and digital cultural heritage preservation.

One of the main features and strengths of RSTB is its ability to handle images of different sizes and resolutions efficiently. We examine our approach with pretrained models according to a software strategy, which is the ImageNet model. The tests are then conducted by sampling 2D images from benchmark datasets (Set5[35], Set14[36], BSD100[37]). Quantitative comparison results between our model (UIR) and other state-of-the-art methods (Bicubic [38], NE+LLE [39], ANR [40], KK [41], SRCNN [42] and SwinIR [54]) for $\times 2$ and $\times 4$ sampling sequentially through look (PSNR [43], SSIM [44]) metric results. Quantitative comparison of the performance of our method (UIR) results on the PSNR (dB) and SSIM metrics compared with those of the other methods. The proposed image processing method is trained and tested on three large-scale datasets: Set5, Set14, and BSD100 fit pretrained ImageNet models. Compared with the state-of-the-art methods, the results of the visual evaluation of our proposed approach (UIR) on images from the test datasets (Set5, Set14, and BSD100) revealed higher resolution and a rougher texture surface with more details.

2. RELATED WORKS

Image recovery is the process of reconstructing high-quality image content from a degraded version [14]. 2D image reconstruction approaches aim to remove the effects of deterioration and convert the two-dimensional image into a state that is close or similar to its true meaning and original dimensions that were captured by the usual lenses [15]. In turn, these algorithms work to reduce the effects that change the basic tilings of the image, remove the defects resulting from the causes, and restore an appropriate shape close to or identical to its original perspective, such as motion blur, noise, camera out-of-focus, lens errors, and sensor noise. Wuttinan et al. [16] proposed a fast data restoration system based on deep learning algorithms by applying the adversarial network (GAN) principle, called the licence plate recovery GAN (LPRGAN). The design employs a proposed encoder–decoder style inspired by autoencoders supported by dual classification networks. This style is suitable for problem-specific learning, as strong contextual information can be retrieved from the reduced representations. Wenbo Li et al. [17] presented an analytical approach to design analysis techniques for ultrahigh-resolution models aimed at efficient image upscaling from HD to 4K. This model presents an accurate description of a precise technique that aims to increase image efficiency through the reconstruction of its details by restoring the high frequencies to their characteristics by reducing the depth maps of the target images by analysing them simultaneously while maintaining their high-accuracy recovery. Delin Liu et al. used terahertz time-domain spectroscopy (THz-TDS) for full-field stress measurement and added it to the superresolution convolutional neural network (SRCNN) method to obtain a high spatial resolution stress field. Modulation models are created from planar voltage states to terahertz TDS signals. A large number of simulated sentences are obtained to train the SRCNN model. The numerical and physical stress fields are mapped via a trained SRCNN model [18]. Yu Cao et al. [19] proposed a novel image enhancement architecture called SR-MRI, which attempts to improve the quality of low-resolution neural images in combination with a real ESRGAN deep learning model. 3T-MRI and 7T-MRI were connected into the same analysis range; then, several evaluation indices, such as Burner, SMD, SMD2, variance, Vollath, entropy, and NIQE, were systematically compared. The experimental results show that the SR-

MRI framework largely recovers the edge, subtle and texture features of low-resolution neural images. Yinggan Tan et al. [20] proposed a new SISR method based on the Wasserstein GAN, which uses the Wasserstein metric to train more stable GANs. To further enhance the superresolution performance and achieve stability during the training steps, two modifications were made to the original WGAN. First, a gradient penalty is introduced to replace weight cutting. Second, create a residual block network with a "preactivation" weight layer in the WGAN's generator. Ziwei Luo et al. [21] proposed improved kernel estimation and kernel-based high-resolution image restoration. Two new modules are reformulated to address the resulting degradation of the superresolution blind images. Standardizing learning for a fixed kernel and all images reduces the kernel weights sufficiently on the basis of the inputs, the most expensive of which is to generate a stronger kernel [61-64]. A deep least squares filtering engine is then applied to generate clean features from the reconstructed and estimated kernels. The defused features and low-input image features are then fed into a dual-path structured SR network to recreate the final high-resolution result [65-67].

3. METHOD

Our approach (UIR), as shown in Figure 1, aims to reconstruct the basic properties of features in single low-resolution (RGB) 2D image ILRs, using convolutional neural networks (CNNs) added to conventional algorithms [1] down to an ultrasuper-resolution 2D image LSR. This scale is close to the high-resolution image and sharpens surface details.

CNNs are powerful image-processing algorithms that can enhance image quality, making images more apparent and visually appealing [22]. Combining multiple CNNs for image enhancement has several advantages. By using multiple CNNs, the strengths of each model can be exploited to achieve better results. Furthermore, a combination of CNNs can help overcome the limitations of individual models, such as overfitting or underfitting [23]. The upscaling method is then applied to the vector patches to create HR images. This process involves various techniques, such as B. Histogram manipulation and extension methods, which are based on generative adversarial networks (GANs) [24]. Furthermore, single-frame deep learning methods involve superresolution, where a method trains end-to-end LR/HR match mapping 2D images directly [25]. Using these techniques, upscaling methods can generate more detailed and sharper HR images than can the original LR images.

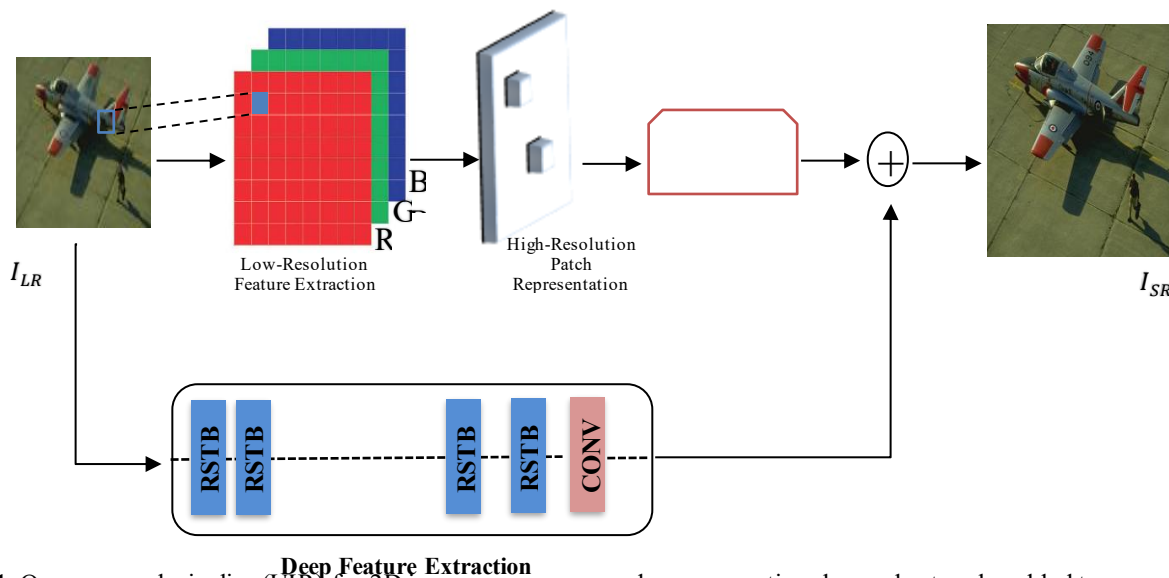


Fig. 1. Our approach pipeline (UIR) for 2D image recovery uses deep conventional neural networks added to conventional algorithms.

In the first stage of our approach, we extract the feature map from a low-resolution image ILR as overlapping high-resolution patches, in which every patch represents a high-dimensional vector by learning deep convolutional neural networks (CNNs) to map between LR/HR 2D images [26]. Patches of feature map extraction by a pretrained model, such as pretrained feature mapping (PFM) [27], are identical to a set of image filters. An is expressed as equation (1).

$$F(ILR) = \max(0, M * ILR + K) \dots \dots \dots (1)$$

M and K represent the image filters. In addition, (ReLU, $\max(0, x)$) [28] is used for a rectified linear unit on the filters. During training, I was required to estimate a parameter of the network. $\Theta = \{M_1, M_2, M_n; K_1, K_2, K_n\}$. This is achieved by lowering the loss between the recovered images $F(ILR, \Theta)$ and the corresponding ground truth high-resolution images IHR via the mean square error loss function (MSE):

$$L(\Theta) = \frac{1}{n} \sum_{i=1}^n \|F(ILR, \Theta) - I_{HR}\|^2 \dots \dots \dots (2)$$

n represents the number of training samples. In the image domain, the upscaling method is applied to every pixel by shifting up features that are extracted to high-resolution vector patches.

In the second stage of our approach, we adopt a logical method for strengthening the basic features of the low-resolution 2D image via deep learning networks to ensure that the missing features of the pixels that occur during the training process are compensated via the residual Swin Transformer block (RSTB). One of the main features and strengths of RSTB is its ability to handle images of different sizes and resolutions efficiently. The a set of the Swin transformer layers uses a multihead self-aware mechanism based on shifted windows, allowing images to be processed on a block basis, which is more memory efficient than processing the entire image at once [29]. The image feature F_1, \dots, F_n is extracted by training the convolutional layer of the STBL. Convolutional layers with spatially invariant filters can improve translation equivariance. Then, the remainder is given an identity-based connection of different blocks with reconstruction modules, allowing aggregation of different feature levels. An is expressed as equation 3.

$$F_i, \text{Extraction} = \text{CLi}(F_i, n) + F_i, 1 \dots \dots \dots (3)$$

$\text{CLi}(F_i, n)$ is an RSTB convolutional layer. Our approach has proven highly effective for integrating deep neural networks and building deep models in the qualitative restoration of 2D image features and has achieved advanced results over some state-of-the-art methods in terms of clarity and accuracy in terms of quality by restoring high-resolution images from low-resolution images, which we will discuss in detail in the next section.

Superresolution models that utilize a residual Swin transformer block (RSTB) commonly use a patch size of 48×48 or 64×64 for the training stage. Our approach (UIR) aims to achieve a balance between computational efficiency and context capture. During the model-training phase, RGB image datasets, as inputs, are divided and transformed into overlapping patches of size 48×48 pixels, with a 50% overlap and a stride of 24 pixels. The validation results demonstrate effective performance on the BSD100, Set14, and Set5 datasets. During inference, overlapping areas are combined with learnable weighted averaging to reduce border artifacts.

The residual Swin Transformer Block (RSTB) for superresolution images consists of several Swin Transformer Layers (STLs) and a residual connection. STL includes LayerNorm (LN), window-based multihead self-attention (W-MSA), or shifted window-based MSA (SW-MSA). The RSTB features six Swin Transformer Layers (STLs) per block for lightweight image restoration, as shown in Figure 2. Easier cross-window connections, the mechanism is switched between the W-MSA and SW-MSA layers in succession. The typical window size for image restoration tasks is 8×8 . Shifting between shift and nonshift windows (window_size=8, shift_size=4) allows for crosswindow connectivity. 6-layer design optimized for SR tasks (vs. 12+ in categorization). For dual-path feature extraction, the transformer path captures long-range relationships via shifted-window self-attention with the CNN path: 3×3 convolutions maintain local texture details and fuse features through a 1×1 convolution with a residual connection. The main procedure explains how RSTB blocks include a convolutional layer to extract and enhance local features:

```

Class RSTB Module ← inputs [No._heads, W_size=8, sht_size=4),
Swin Transformer (ST) Layers ← No._heads=No._heads, W_size=W_size,
for i in range(6) # 6-layer configuration
#Convolutional Enhancemen ← self.conv_block = nn.Sequential mm. Conv2d(dim, dim, 3, padding=1), mm. ReLU(),
Feature Fusion ← self.fusion = nn. Conv2d(2*dim, dim, 1)
    combined = torch.cat([x_trans, p_conv], dim=1)
    out.s = self.fusion(combined) + shortcut.p
return out

```

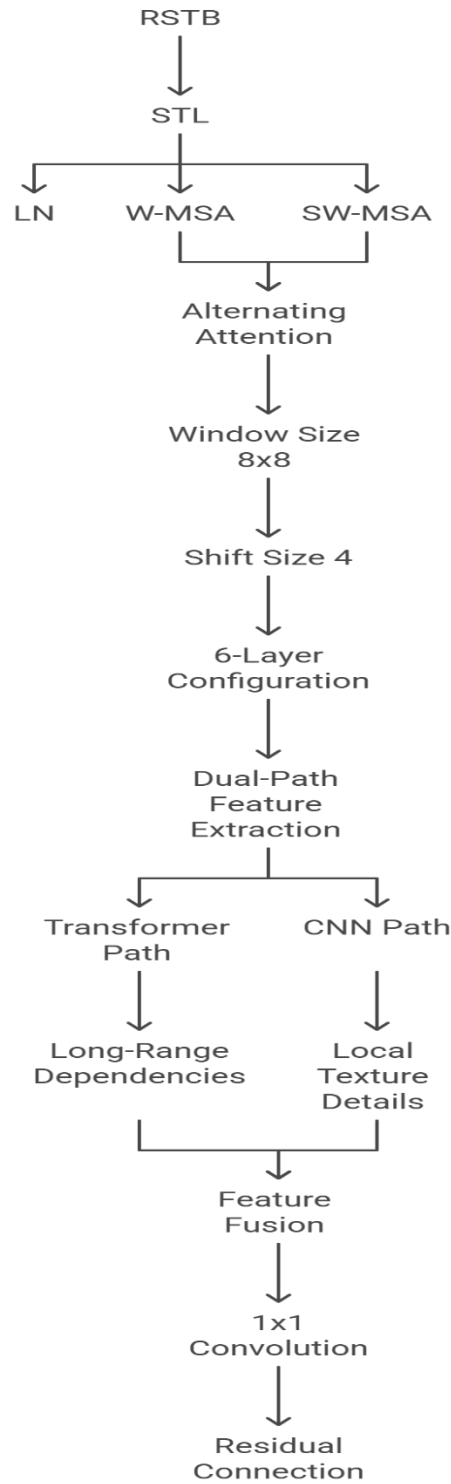


Fig. 2. RSTB architecture used in the UIR approach for image superresolution.

4. EXPERIMENTS

4.1 Training Model

To extract features from low-resolution (SR) images and find high-resolution patch vectors via the ImageNet dataset [30] for pretraining, image superresolution models include selecting a pretraining model, fine-tuning the model on the ImageNet

dataset, and then fine-tuning the model on the target image superresolution dataset [31]. Data augmentation techniques can also be used to increase the quality of the training dataset, leading to better model performance. By using the ImageNet dataset for pretraining image superresolution models, the model can learn to extract high-level features from images, leading to improved image quality and resolution [32]. In addition, ImageNet pretrained models include pretrained deep learning architectures, such as VGG-16, a well-known ImageNet pretrained model [33]. In fact, VGG-16 won first place in ImageNet ILSVRC-2014, making it one of the best-pretrained models for image classification [34]. Researchers can use this open-source pretrained model to create image classification models or improve existing models.

To ensure that the model is tested with more accurate results, we also use the DIV2K dataset, which is often used to pretrain high-resolution image models. The dataset consists of 1000 high-resolution (2K) RGB images with different contents and is used to pretrain DnCNN-based schemes and SVQE models for image superresolution [4]. In a specific experiment, 750 images from this dataset were used for training, with a QP set to 45 for high-resolution images [4]. When synthesizing low-resolution images for different challenge tracks, different types of degradations are considered in addition to standard bicubic downsampling [51-55].

An upscaling factor learns ImageNet-trained first-layer filters of 2 or 4. Interestingly, each kind of filter is learned before it has a specific function. For example, filters *g* and *h* are Laplacian/Gaussian filters, edge detectors with variable orientations, and surface texture extractors, respectively [56-60].

4.2 Results

We must examine our approach via pretrained models according to a software strategy using the Python language, which is the ImageNet model. The tests are then conducted by sampling 2D images from benchmark datasets (Set5 [35], Set14 [36], BSD100 [37]). Tables 1 and 2 show quantitative comparison results between our model (UIR) and state-of-the-art methods (Bicubic [38], NE+LLE [39], ANR [40], KK [41], and SRCNN [42]) for $\times 2$ and $\times 4$ sampling sequentially through look (PSNR [43], SSIM [44]) metric results.

Table 1. The quantitative comparison results of (PSNR (dB)/SSIM) on $\times 2$ upscaling between our approach and state-of-the-art methods.

Method	Scale	Pre-Training Model	Set5		Set14		BSD100	
			PSNR	SSIM	PSNR	SSIM	PSNR	SSIM
Bicubic	2	ImageNet	33.66	0.9299	30.23	0.8687	28.38	0.8524
NE+LLE	2	ImageNet	35.77	0.9490	31.76	0.8993	29.67	0.8886
ANR	2	ImageNet	35.83	0.9499	32.28	0.9056	30.14	0.8966
KK	2	ImageNet	36.20	0.9511	31.80	0.9004	29.72	0.8900
SRCNN	2	ImageNet	36.66	0.9542	32.45	0.9067	30.29	0.8977
SwinIR	2	ImageNet	36.74	0.9639	34.79	0.9412	33.81	0.9016
UIR(our)	2	ImageNet	36.86	0.9739	36.10	0.9656	34.74	0.9893

Table 2. The quantitative comparison results of (PSNR (dB)/SSIM) on $\times 4$ upscaling between our approach and state-of-the-art methods.

Method	Scale	Pre-Training Model	Set5		Set14		BSD100	
			PSNR	SSIM	PSNR	SSIM	PSNR	SSIM
Bicubic	4	ImageNet	28.42	0.8104	26.00	0.7019	24.65	0.6727
NE+LLE	4	ImageNet	29.61	0.8402	26.81	0.7331	25.21	0.7037
ANR	4	ImageNet	29.69	0.8419	27.32	0.7491	25.51	0.7171
KK	4	ImageNet	30.03	0.8541	26.85	0.7352	25.25	0.7060
SRCNN	4	ImageNet	30.49	0.8628	27.50	0.7513	25.60	0.7184
SwinIR	2	ImageNet	32.20	0.8732	27.63	0.7927	25.78	0.8331
UIR(our)	4	ImageNet	34.44	0.8784	27.71	0.8894	26.87	0.9915

A quantitative evaluation of our method's performance (UIR) with respect to state-of-the-art approaches yields results in terms of the PSNR (dB) and SSIM metrics, as demonstrated in Tables 1 and 2. The proposed image processing method is trained and tested on three large-scale datasets: Set5, Set14, and BSD100 fit pretrained ImageNet models. The PSNR specifications are 36.86 dB, 36.10 dB, and 34.74 dB at the $\times 2$ image scale. Our method also outperforms other 2D image processing methods in quantitatively evaluating the SSIM metric, yielding the best quantitative results of 0.9739, 0.9656, and 0.9893. The evaluation is based on the PSNR (dB) and SSIM metrics, and the best values are shown in the comparison in Table 1. Additionally, the results of the proposed approach are more advanced than those of state-of-the-art methods when the scale of 2D images is increased to $\times 4$ when the ImageNet pretrained model is trained. The quantitative evaluation results are presented in Table 2. The PSNR values are 34.44, 27.71, and 26.87, and the SSIM values are 0.97849, 0.8894, and 0.9915. We notice through the curves in Figure 3 and Figure 4 the accuracy achieved by our method through the high values obtained compared with the values created by other methods.

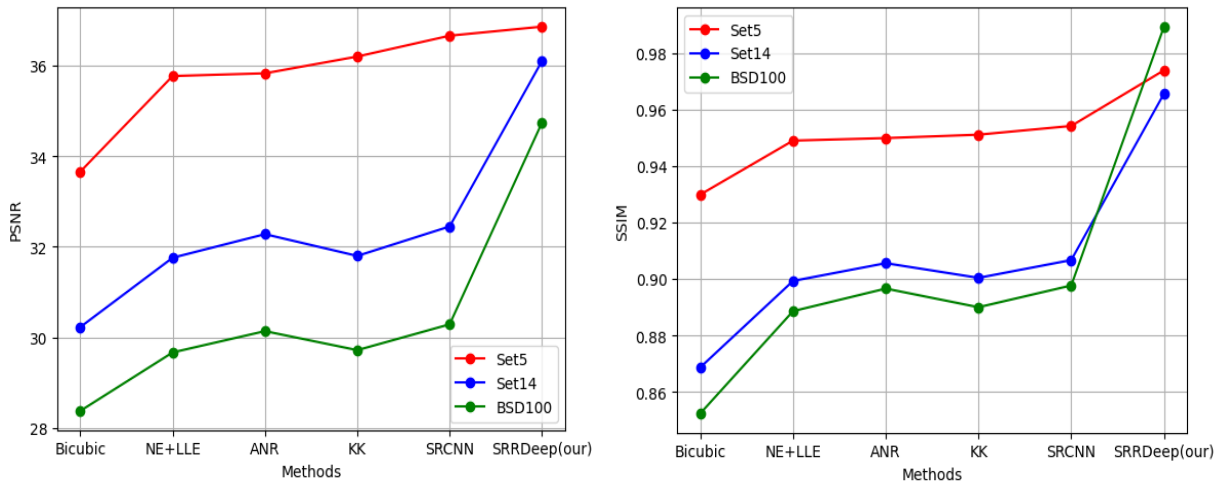
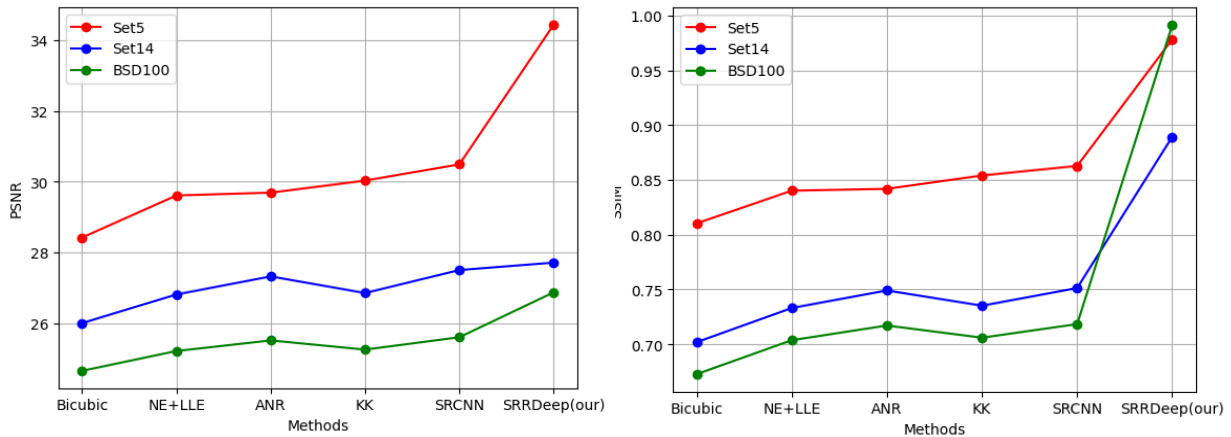


Fig. 3. PSNR(dB)/SSIM curve results of UIR compared with those of the other methods on the x2 magnified images of the Set5, Set14 and DSB100 datasets.

Fig. 4. PSNR(dB)/SSIM curve results of UIR compared with those of the other methods on the x2 magnified images of



the Set5, Set14 and DSB100 datasets.

Our RSTB design is more sophisticated owing to shifted-window attention, with 301 GMACs for 720p input (compared with SwinIR's 235). The inference latency of the RSTB algorithm reaches 36.10 dB PSNR on Set14 at 143 ms (V200 GPU), which is 42% slower than that of SwinIR but 1.31 dB greater in fidelity.

As shown in Figures 5, 6, and 7, the results of the visual evaluation of our UIR method compared with the state-of-the-art methods on images from the test datasets (Set5, Set14, and BSD100) revealed higher resolution and a rougher texture surface with more details. Accordingly, the method adopted in this approach has achieved superresolution 2D single-image ISR from low-resolution image ILR that is close to natural image I_{HR} .

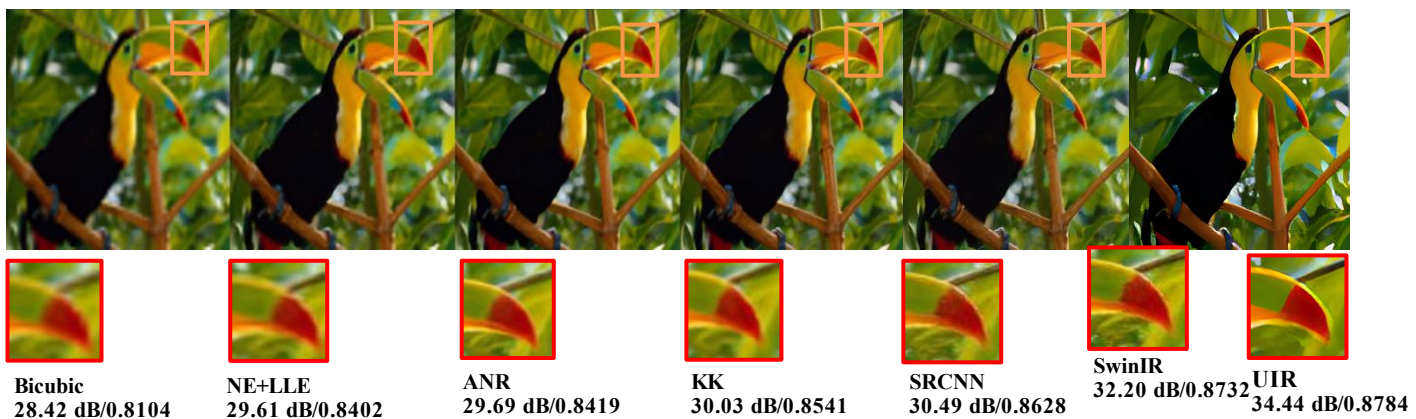


Fig. 5. Visual evaluation of bird images in the Set5 dataset (x4) methods.

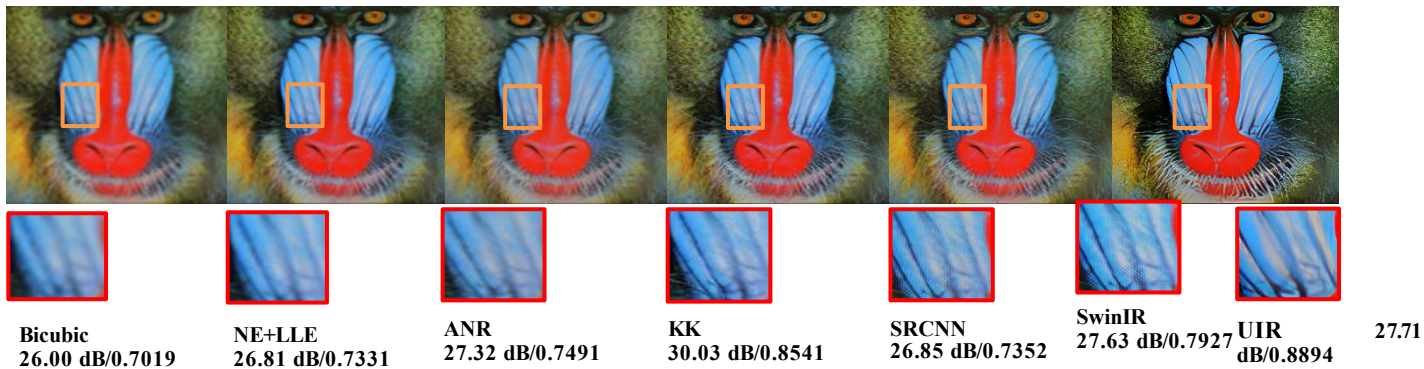


Fig. 6. Visual evaluation of baboon images in the Set14 dataset (x4) methods.



Fig. 7. Visual evaluation of 3096 images in the BSD100 dataset (x4).

5. CONCLUSION

We introduced a deep learning strategy for single-image recovery called superresolution (SR). A high-dimensional vector patch is identified through extracting a feature map from low-resolution image ILR overlapping high-resolution patches by learning deep convolutional neural networks (CNNs) to map between LR/HR 2D images. In addition, the essential features of low-resolution 2D images are augmented via deep learning networks to ensure that residual Swin Transformer-Block (RSTB) is used to compensate for pixel-missing features that occur during training. This method has achieved superior performance in image upscaling and high-resolution 2D image texture surface reconstruction. Thus, this deep method can be used to recover rare, low-resolution images that are found on web engines, such as archeological images or images that extend back to the past century and that were taken before the current technological advancements. Through experimental settings, we can see a genuine and concrete benefit of contemporary approaches over their predecessors. However, severe failures persist, necessitating efforts to close the gap between quantitative tests and tangible, real-world outcomes. This necessitates reducing the complexity of deterioration and enhancing the perceived consistency of recovered pictures. All research efforts and improved outcomes prioritize robustness and the reduction of physical degradation models, which is a promising direction.

Conflicts of interest

The authors declare no conflicts of interest.

Funding

This work was supported by the Deanship of Scientific Research, Vice Presidency for Graduate Studies and Scientific Research, King Faisal University, Saudi Arabia KFU252878

Acknowledgement

The authors extend appreciation to the institution for their unwavering support and encouragement during this research.

References

- [1] S. Rizvi, J. Cao, and Q. Hao, "Deep learning based projector defocus compensation in single-pixel imaging," *Opt. Express*, vol. 28, no. 17, p. 25134, 2020, doi: 10.1364/oe.397783.
- [2] C. Belthangady and L. A. Royer, "Applications, promises, and pitfalls of deep learning for fluorescence image reconstruction," *Nat. Methods*, vol. 16, no. 12, pp. 1215–1225, 2019, doi: 10.1038/s41592-019-0458-z.
- [3] F. Zhang, X. Wang, T. Sun, and X. Xu, "SE-DCGAN: a New Method of Semantic Image Restoration," *Cognit. Comput.*, vol. 13, no. 4, pp. 981–991, 2021, doi: 10.1007/s12559-021-09877-y.
- [4] M. V. Conde, F. Vasluianu, J. Vazquez-Corral, and R. Timofte, "Perceptual Image Enhancement for Smartphone Real-Time Applications," *Proc. - 2023 IEEE Winter Conf. Appl. Comput. Vision, WACV 2023*, pp. 1848–1858, 2023, doi: 10.1109/WACV56688.2023.00189.
- [5] J. Yang, J. Wright, T. S. Huang, and Y. Ma, "Image super-resolution via sparse representation," *IEEE Trans. Image Process.*, vol. 19, no. 11, pp. 2861–2873, 2010, doi: 10.1109/TIP.2010.2050625.
- [6] Z. Shao, L. Wang, Z. Wang, and J. Deng, "Remote Sensing Image Super-Resolution Using Sparse Representation and Coupled Sparse Autoencoder," *IEEE J. Sel. Top. Appl. Earth Obs. Remote Sens.*, vol. 12, no. 8, pp. 2663–2674, 2019, doi: 10.1109/JSTARS.2019.2925456.
- [7] Z. Cui, H. Chang, S. Shan, B. Zhong, and X. Chen, "Deep network cascade for image super-resolution," *Lect. Notes Comput. Sci. (including Subser. Lect. Notes Artif. Intell. Lect. Notes Bioinformatics)*, vol. 8693 LNCS, no. PART 5, pp. 49–64, 2014, doi: 10.1007/978-3-319-10602-1_4.
- [8] C. Liu, H. Y. Shum, and W. T. Freeman, "Face hallucination: Theory and practice," *Int. J. Comput. Vis.*, vol. 75, no. 1, pp. 115–134, 2007, doi: 10.1007/s11263-006-0029-5.
- [9] N. Meng, H. K. H. So, X. Sun, and E. Y. Lam, "High-Dimensional Dense Residual Convolutional Neural Network for Light Field Reconstruction," *IEEE Trans. Pattern Anal. Mach. Intell.*, vol. 43, no. 3, pp. 873–886, 2021, doi: 10.1109/TPAMI.2019.2945027.
- [10] Q. Wu *et al.*, "An Arbitrary Scale Super-Resolution Approach for 3D MR Images via Implicit Neural Representation," *IEEE J. Biomed. Heal. Informatics*, vol. 27, no. 2, pp. 1004–1015, 2023, doi: 10.1109/JBHI.2022.3223106.
- [11] R. S. Mousa and R. Shehab, "Applying risk analysis for determining threats and countermeasures in workstation domain," *Journal of Cyber Security and Risk Auditing*, vol. 2025, no. 1, pp. 12–21, 2025.
- [12] H. Ding *et al.*, "ContransGAN: Convolutional Neural Network Coupling Global Swin-Transformer Network for High-Resolution Quantitative Phase Imaging with Unpaired Data," *Cells*, vol. 11, no. 15, 2022, doi: 10.3390/cells11152394.
- [13] B. Hardiansyah and Y. Lu, "Single image super-resolution via multiple linear mapping anchored neighborhood regression," *Multimed. Tools Appl.*, vol. 80, no. 19, pp. 28713–28730, 2021, doi: 10.1007/s11042-021-11062-0.
- [14] M. Zhang and C. Desrosiers, "High-quality Image Restoration Using Low-Rank Patch Regularization and Global Structure Sparsity," *IEEE Trans. Image Process.*, vol. 28, no. 2, pp. 868–879, 2019, doi: 10.1109/TIP.2018.2874284.
- [15] T. V. Dang, G. H. Yu, H. T. Nguyen, H. T. Vo, J. H. Lee, and J. Y. Kim, "Convolutional Neural Network-based image retrieval with degraded sample," *ACM Int. Conf. Proceeding Ser.*, pp. 86–91, 2020, doi: 10.1145/3426020.3426041.
- [16] W. Sereethavekul and M. Ekpanyapong, "Adaptive Lightweight License Plate Image Recovery using Deep Learning based on Generative Adversarial Network," *IEEE Access*, 2023, doi: 10.1109/ACCESS.2023.3255641.
- [17] W. Li, K. Zhou, L. Qi, L. Lu, and J. Lu, "Best-Buddy GANs for Highly Detailed Image Super-resolution," *Proc. 36th AAAI Conf. Artif. Intell. AAAI 2022*, vol. 36, pp. 1412–1420, 2022, doi: 10.1609/aaai.v36i2.20030.
- [18] S. Ootom, "Risk auditing for Digital Twins in cyber physical systems: A systematic review," *Journal of Cyber Security and Risk Auditing*, vol. 2025, no. 1, pp. 22–35, 2025.
- [19] Y. Cao, H. Kuai, and G. Peng, "Enhancing the MR Neuroimaging by Using the Deep Super-Resolution Reconstruction," *Lect. Notes Comput. Sci. (including Subser. Lect. Notes Artif. Intell. Lect. Notes Bioinformatics)*, vol. 13406 LNAI, pp. 184–194, 2022, doi: 10.1007/978-3-031-15037-1_16.
- [20] Y. Tang, C. Liu, and X. Zhang, "Single image super-resolution using Wasserstein generative adversarial network with gradient penalty," *Pattern Recognit. Lett.*, vol. 163, pp. 32–39, 2022, doi: 10.1016/j.patrec.2022.09.012.
- [21] Z. Luo, H. Huang, L. Yu, Y. Li, H. Fan, and S. Liu, "Deep Constrained Least Squares for Blind Image Super-Resolution," *Proc. IEEE Comput. Soc. Conf. Comput. Vis. Pattern Recognit.*, vol. 2022-June, pp. 17621–17631, 2022, doi: 10.1109/CVPR52688.2022.01712.
- [22] X. Liu, Y. Yang, Y. Zhong, D. Xiong, and Z. Huang, "Super-Pixel Guided Low-Light Images Enhancement with Features Restoration," *Sensors*, vol. 22, no. 10, 2022, doi: 10.3390/s22103667.
- [23] L. C. Ngugi, M. Abelwahab, and M. Abo-Zahhad, "Recent advances in image processing techniques for automated leaf pest and disease recognition – A review," *Inf. Process. Agric.*, vol. 8, no. 1, pp. 27–51, 2021, doi: 10.1016/j.inpa.2020.04.004.

- [24] H. Alqahtani, M. Kavakli-Thorne, and G. Kumar, "Applications of Generative Adversarial Networks (GANs): An Updated Review," *Arch. Comput. Methods Eng.*, vol. 28, no. 2, pp. 525–552, 2021, doi: 10.1007/s11831-019-09388-y.
- [25] Y. Guo *et al.*, "Closed-loop matters: Dual regression networks for single image super-resolution," *Proc. IEEE Comput. Soc. Conf. Comput. Vis. Pattern Recognit.*, pp. 5406–5415, 2020, doi: 10.1109/CVPR42600.2020.00545.
- [26] M. Zhang, W. Li, Q. Du, L. Gao, and B. Zhang, "Feature Extraction for Classification of Hyperspectral and LiDAR Data Using Patch-to-Patch CNN," *IEEE Trans. Cybern.*, vol. 50, no. 1, pp. 100–111, 2020, doi: 10.1109/TCYB.2018.2864670.
- [27] Q. Wan, L. Gao, X. Li, and L. Wen, "Unsupervised Image Anomaly Detection and Segmentation Based on Pre-Trained Feature Mapping," *IEEE Trans. Ind. Informatics*, 2022, doi: 10.1109/TII.2022.3182385.
- [28] V. Nair and G. E. Hinton, "Rectified Linear Units Improve Restricted Boltzmann Machines," *J. Appl. Biomech.*, vol. 33, no. 5, pp. 384–387, 2017.
- [29] W. Xing and K. Egiazarian, "Residual Swin Transformer Channel Attention Network for Image Demosaicing," *Proc. - Eur. Work. Vis. Inf. Process. EUVIP*, vol. 2022-Sept, 2022, doi: 10.1109/EUVIP53989.2022.9922679.
- [30] E. Denton, A. Hanna, R. Amironesei, A. Smart, and H. Nicole, "On the genealogy of machine learning datasets: A critical history of ImageNet," *Big Data Soc.*, vol. 8, no. 2, 2021, doi: 10.1177/20539517211035955.
- [31] H. Chen *et al.*, "Real-world single image super-resolution: A brief review," *Inf. Fusion*, vol. 79, pp. 124–145, 2022, doi: 10.1016/j.inffus.2021.09.005.
- [32] S. Ayas and M. Ekinici, "Microscopic image superresolution using deep convolutional neural networks," *Multimed. Tools Appl.*, vol. 79, no. 21–22, pp. 15397–15415, 2020, doi: 10.1007/s11042-019-7397-7.
- [33] A. T. Kabakus and P. Erdogmus, "An experimental comparison of the widely used pre-trained deep neural networks for image classification tasks towards revealing the promise of transfer-learning," *Concurr. Comput. Pract. Exp.*, vol. 34, no. 24, 2022, doi: 10.1002/cpe.7216.
- [34] S. Tammina, "Transfer learning using VGG-16 with Deep Convolutional Neural Network for Classifying Images," *Int. J. Sci. Res. Publ.*, vol. 9, no. 10, p. p9420, 2019, doi: 10.29322/ijrsp.9.10.2019.p9420.
- [35] E. Agustsson and R. Timofte, "NTIRE 2017 Challenge on Single Image Super-Resolution: Dataset and Study," *IEEE Comput. Soc. Conf. Comput. Vis. Pattern Recognit. Work.*, vol. 2017-July, pp. 1122–1131, 2017, doi: 10.1109/CVPRW.2017.150.
- [36] Z. Lu and Y. Chen, "Single image super-resolution based on a modified U-net with mixed gradient loss," *Signal, Image Video Process.*, vol. 16, no. 5, pp. 1143–1151, 2022, doi: 10.1007/s11760-021-02063-5.
- [37] D. Chira, I. Haralampiev, O. Winther, A. Dittadi, and V. Liévin, "Image Super-Resolution with Deep Variational Autoencoders," pp. 395–411, 2023, doi: 10.1007/978-3-031-25063-7_24.
- [38] Z. Huang and L. Cao, "Bicubic interpolation and extrapolation iteration method for high resolution digital holographic reconstruction," *Opt. Lasers Eng.*, vol. 130, 2020, doi: 10.1016/j.optlaseng.2020.106090.
- [39] K. Cheng, J. Du, H. Zhou, D. Zhao, and H. Qin, "Image super-resolution based on half quadratic splitting," *Infrared Phys. Technol.*, vol. 105, 2020, doi: 10.1016/j.infrared.2020.103193.
- [40] R. Timofte, V. De Smet, and L. Van Gool, "A+: Adjusted anchored neighborhood regression for fast super-resolution," *Lect. Notes Comput. Sci. (including Subser. Lect. Notes Artif. Intell. Lect. Notes Bioinformatics)*, vol. 9006, pp. 111–126, 2015, doi: 10.1007/978-3-319-16817-3_8.
- [41] D. C., L. C., H. K., and T. X., "Image super-resolution using deep convolutional networks," *IEEE Trans. Pattern Anal. Mach. Intell.*, vol. 38, no. 2, pp. 295–307, 2016.
- [42] Y. Da Wang, R. T. Armstrong, and P. Mostaghimi, "Enhancing Resolution of Digital Rock Images with Super Resolution Convolutional Neural Networks," *J. Pet. Sci. Eng.*, vol. 182, 2019, doi: 10.1016/j.petrol.2019.106261.
- [43] D. R. I. M. Setiadi, "PSNR vs SSIM: imperceptibility quality assessment for image steganography," *Multimed. Tools Appl.*, vol. 80, no. 6, pp. 8423–8444, 2021, doi: 10.1007/s11042-020-10035-z.
- [44] I. Bakurov, M. Buzzelli, R. Schettini, M. Castelli, and L. Vanneschi, "Structural similarity index (SSIM) revisited: A data-driven approach," *Expert Syst. Appl.*, vol. 189, 2022, doi: 10.1016/j.eswa.2021.116087.
- [45] A. S. Rasheed, R. H. Finjan, A. A. Hashim, and M. M. Al-Saeedi, "3D face creation via 2D images within blender virtual environment," *Indones. J. Electr. Eng. Comput. Sci.*, vol. 21, no. 1, pp. 457–464, 2021, doi: 10.11591/ijeecs.v21.i1.pp457-464.
- [46] A. S. Rasheed, M. Jabberi, T. M. Hamdani, and A. M. Alimi, "Exploring the Potential of High-Resolution Drone Imagery for Improved 3D Human Avatar Reconstruction: A Comparative Study with Mobile Images," *Lect. Notes Comput. Sci. (including Subser. Lect. Notes Artif. Intell. Lect. Notes Bioinformatics)*, vol. 14403 LNCS, pp. 167–181, 2024, doi: 10.1007/978-981-97-0376-0_13.
- [47] A. S. Rasheed, A. H. Omran, and Y. M. Abid, "Development of Drone-Based Human Rescue Strategies Using Virtual Reality," *Iraqi J. Sci.*, vol. 65, no. 6, pp. 3550–3560, 2024, doi: 10.24996/ij.s.2024.65.6.45.
- [48] A. S. Rasheed and A. Hamza Omran, "Embedded Deep Learning to Improve the Performance of Approaches for Extinct Heritage Images Denoising," *Iraqi J. Comput. Sci. Math.*, vol. 5, no. 3, pp. 526–534, 2024, doi: 10.52866/ijcsm.2024.5.03.033.
- [49] A. Salim Rasheed, M. Jabberi, T. M. Hamdani, and A. M. Alimi, "PIXGAN-Drone: 3D Avatar of Human Body Reconstruction From Multi-View 2D Images," *IEEE Access*, vol. 12, pp. 74762–74776, 2024, doi: 10.1109/ACCESS.2024.3404554.
- [50] R. H. Finjan and A. S. Rasheed, "Iraqi Multi-style License Plate Recognition System using Efficient Dets Model",

- [Online]. Available: www.ijlera.com
- [51] A. A. Almuqren, "Cybersecurity threats, countermeasures and mitigation techniques on the IoT: Future research directions," *Journal of Cyber Security and Risk Auditing*, vol. 1, no. 1, pp. 1–11, 2025.
 - [52] R. Almanasir, D. Al-solomon, S. Indrawes, M. Almaiah, U. Islam, and M. Alsha'r'e, "Classification of threats and countermeasures of cloud computing," *Journal of Cyber Security and Risk Auditing*, vol. 2025, no. 2, pp. 27–42, 2025.
 - [53] Almedires, M. A., Elkhail, A., & Amin, M. (2025). Adversarial Attack Detection in Industrial Control Systems Using LSTM-Based Intrusion Detection and Black-Box Defense Strategies. *Journal of Cyber Security and Risk Auditing*, 2025(3), 4-22.
 - [54] S. Ang, M. Ho, S. Huy, and M. Janarthanan, "Utilizing IDS and IPS to improve cybersecurity monitoring process," *Journal of Cyber Security and Risk Auditing*, vol. 2025, no. 3, pp. 77–88, 2025.
 - [55] N. Frederick and A. Ali, "Enhancing DDoS attack detection and mitigation in SDN using advanced machine learning techniques," *Journal of Cyber Security and Risk Auditing*, vol. 2024, no. 1, pp. 23–37, 2024.
 - [56] A. Aldossary, T. Algirim, I. Almubarak, and K. Almuish, "Cyber security in data breaches," *Journal of Cyber Security and Risk Auditing*, vol. 2024, no. 1, pp. 14–22, 2024.
 - [57] A. Ali and R. Shehab, "A systematic review of security risk management for banking systems," *Journal of Cyber Security and Risk Auditing*, vol. 2023, no. 1, pp. 49–72, 2023.
 - [58] A. Davarasan, J. Samual, K. Palansundram, and A. Ali, "A comprehensive review of machine learning approaches for Android malware detection," *Journal of Cyber Security and Risk Auditing*, vol. 2024, no. 1, pp. 38–60, 2024.
 - [59] B. Almelehy, M. Ahmad, G. Nassreddine, M. Maayah, and A. Achanta, "Analytical analysis of cyber threats and defense mechanisms for web application security," *Journal of Cyber Security and Risk Auditing*, vol. 2025, no. 3, pp. 57–76, 2025.
 - [60] A. Alshuaibi, M. Almaayah, and A. Ali, "Machine learning for cybersecurity issues: A systematic review," *Journal of Cyber Security and Risk Auditing*, vol. 2025, no. 1, pp. 36–46, 2025.
 - [61] A. Ali, "Adaptive and Context-Aware Authentication Framework Using Edge AI and Blockchain in Future Vehicular Networks," *STAP Journal of Security Risk Management*, vol. 2024, no. 1, pp. 45–56, 2024, doi: 10.63180/jsrm.thestap.2024.1.3.
 - [62] S. R. Addula, S. Norozpour, and M. Amin, "Risk Assessment for Identifying Threats, vulnerabilities and countermeasures in Cloud Computing," *Jordanian Journal of Informatics and Computing*, vol. 2025, no. 1, pp. 38–48, 2025, doi: 10.63180/jjic.thestap.2025.1.5.
 - [63] M. A. Al-Shareeda, L. B. Najm, A. A. Hassan, S. Mushtaq, and H. A. Ali, "Secure IoT-based smart agriculture system using wireless sensor networks for remote environmental monitoring," *STAP Journal of Security Risk Management*, vol. 2024, no. 1, pp. 56–66, 2024.
 - [64] M. Alshinwan, A. G. Memon, M. C. Ghanem, and M. Almaayah, "Unsupervised text feature selection approach based on improved Prairie dog algorithm for the text clustering," *Jordanian Journal of Informatics and Computing*, vol. 2025, no. 1, pp. 27–36, 2025.
 - [65] M. Almaayah and R. B. Sulaiman, "Cyber Risk Management in the Internet of Things: Frameworks, Models, and Best Practices," *STAP Journal of Security Risk Management*, vol. 2024, no. 1, pp. 3–23, 2024.
 - [66] H. Albinhamad, A. Alotibi, A. Alagham, M. Almaiah, and S. Salloum, "Vehicular Ad-hoc Networks (VANETs): A key enabler for smart transportation systems and challenges," *Jordanian Journal of Informatics and Computing*, vol. 2025, no. 1, pp. 4–15, 2025.
 - [67] S. Alsahaim and M. Maayah, "Analyzing Cybersecurity Threats on Mobile Phones," *STAP Journal of Security Risk Management*, vol. 2023, no. 1, pp. 3–19, Aug. 2023.